Carbohydrate Polymers 89 (2012) 821–829

Contents lists available at SciVerse ScienceDirect

Carbohydrate Polymers

journal homepage: www.elsevier.com/locate/carbpol

Synthesis of superparamagnetic bare Fe_3O_4 nanostructures and core/shell (Fe_3O_4/alginate) nanocomposites

Manish Srivastava [a,e], Jay Singh [b], Madhu Yashpal [c], Dinesh Kumar Gupta [d], R.K. Mishra [a], Shipra Tripathi [f], Animesh K. Ojha [a,*]

[a] Department of Physics, Motilal Nehru National Institute of Technology, Allahabad, Allahabad 211004, India
[b] Department of Science and Technology Centre on Biomolecular Electronics Biomedical Instrumentation Section, National Physical Laboratory, Dr. K.S. Krishnan Marg, New Delhi 110012, India
[c] Electron Microscope Facility, Department of Anatomy, Institute of Medical Sciences, Banaras Hindu University, Varanasi 221005, India
[d] Department of Chemistry, Motilal Nehru National Institute of Technology, Allahabad, Allahabad 211004, India
[e] Department of Physics, Dehradun Institute of Technology (DIT) School of engineering, Greater Noida 248001, India
[f] Department of Chemistry, School of Basic and Applied Sciences, Galgotias University, Gautam Budha Nagar 201306, India

ARTICLE INFO

Article history:
Received 12 July 2011
Received in revised form 23 February 2012
Accepted 6 April 2012
Available online 13 April 2012

Keywords:
Magnetic NPs
Composites
Biomedical
Alginate
Core–shell

ABSTRACT

In this article we report about the synthesis of superparamagnetic bare Fe_3O_4 nanostructures and core/shell (Fe_3O_4/alginate) nanocomposites by simple low-temperature based method at pH values 5, 9, and 14. The structural morphology and magnetic behavior of Fe_3O_4 nanostructures and core/shell (Fe_3O_4/alginate) nanocomposites (Fe_3O_4/alg NCs) have been investigated by X-ray diffractometer (XRD), Fourier transform infrared spectroscopy (FT-IR), Raman spectroscopy (RS), ultraviolet–visible (UV–vis) spectroscopy, transmission electron microscopy (TEM), energy dispersive X-ray spectroscopy (EDX) and vibrating sample magnetometer (VSM). The particle size was calculated by TEM measurements and it turns out to be ~10 nm and ~14 nm for bare Fe_3O_4 nanoparticle and Fe_3O_4/alg NCs with core/shell structure, respectively. The magnetic properties of the synthesized products were found to be function of pH at which the synthesis has been done. The synthesized Fe_3O_4 nanoparticle and Fe_3O_4/alg NCs were found to be superparmagnetic in nature at room temperature. We observed that the value of saturation magnetization in case of Fe_3O_4/alg NCs decreases by increasing the pH value.

1. Introduction

Currently, the investigations on magnetic nanoparticles (MNPs) have attracted considerable attention to the scientist due to its application in various fields such as physics, medicine, biology and materials science. Particularly, superparamagnetic materials play an important role in biomedical applications including magnetic resonance imaging for clinical diagnosis, magnetic drug targeting, hyperthermia anti-cancer strategy (Gupta & Gupta, 2005; Kim et al., 2008; Qu, Liu, Wang, & Hong, 2010) and enzyme immobilization (Singh, Kalita, Singh, & Malhotra, 2011; Singh, Srivastava, Dutta, & Dutta, 2011). Magnetite (Fe_3O_4) and maghemite (γ-Fe_2O_3) are the most commonly used magnetic carriers for a variety of biomedical applications (Liu et al., 2007). Among the various types of magnetic materials, the magnetic–polymer composites represent a class of functional materials where magnetic NPs are embedded in polymer matrixes. Recently, a considerable number of studies have been done on magnetic–polymer nanocomposites such as; PVP-coated Fe_3O_4 (Liu et al., 2007), Fe_3O_4–chitosan and α-Fe_2O_3 NPs (Li, Jiang, Huang, Ding, & Chen, 2008; Singh, Kalita, et al., 2011; Singh, Srivastava, et al., 2011), tyrosinase biosensor based on Fe_3O_4 NPs–chitosan nanocomposite (Wang, Bao, Yang, Chen, 2008), barium alginate caged Fe_3O_4/C_{18} magnetic NPs (Zhang, Shi, Yang, De, & Wang, 2010), polyaniline-coated nano-Fe_3O_4/carbon nanotube composite as the protein digestion (Wang, Tan, Zhao, & Liu, 2008), Fe_3O_4/PPy/P(MAA-co-AAm) trilayered composite (Luo et al., 2010), Fe_3O_4-PVA nanocomposites (Liu, Hu, Liu, Liu, & Chen, 2008), polyaniline/nano-Fe_3O_4/composites (Xiao, Tan, Ji, & Xue, 2007), polymer–Fe_3O_4 nanocomposites (Yang, Brown, Kempel, & Kofinas, 2008), PEI modified Fe_3O_4/Au NPs (Sun, Zhu, Zhang, Zhang, & Wang, 2010), alginic acid–Fe_3O_4/nanocomposite (Unal, Toprak, Durmus, Sözeri, & Baykal, 2010). The biocompatibility of magnetic materials can be tuned by variety of the polymer coating.

Among the various types of polymers, alginate has attracted intense attention as an important class of biomaterial. It exhibits unique properties such as; biocompatibility, inexpensiveness, mild encapsulation process at room temperature and a relatively inert hydrogel environment within the matrix. Moreover, one of the

* Corresponding author. Tel.: +91 5322271289.
E-mail addresses: animesh@mnnit.ac.in, animesh198@gmail.com (A.K. Ojha).

0144-8617/$ – see front matter © 2012 Elsevier Ltd. All rights reserved.
http://dx.doi.org/10.1016/j.carbpol.2012.04.016

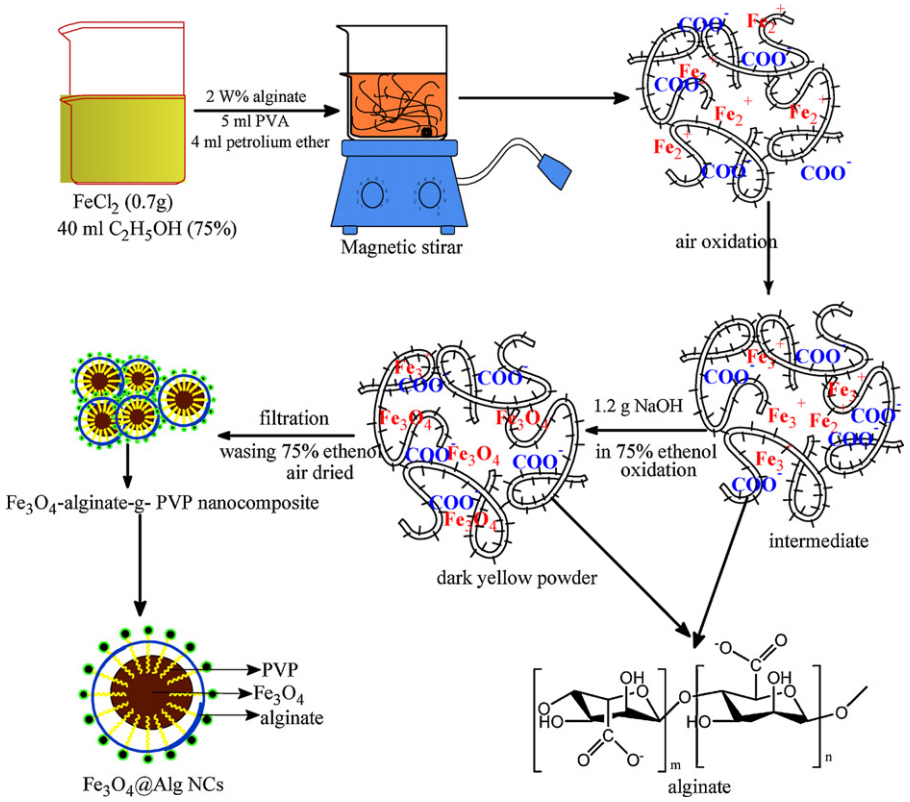

Fig. 1. Schematic diagram show the synthesis method of the Fe_3O_4/alg NCs by in situ co-precipitation method.

unique properties of alginate is its simple gelation with divalent cations like Ca^{2+} which is ionically crosslink carboxylate groups in the G-block of alginate and has been extensively investigated for many biomedical applications such as; cell transplantation matrices, tissue engineering and drug delivery vehicles (Liu et al., 2009). Another imperative approach related to the in situ gel properties of alginate is represented by its possible application in wound dressing because of the presence of calcium ions in the exudates. Alginate can also be mixed with other natural polymers, such as; gelatin and chitosan to produce physical gels. The polymer matrix can be loaded with antibiotics. Alginate can also be chemically modified into low molecular weight oligomers which would be then cross-linked with a biodegradable spacer to form biodegradable hydrogels (Pielesz, 2007).

Alginate is a well-known naturally occurring polysaccharide which is composed of guluronic (G) and mannuronic (M) acid residues (1,4-linked α-L-guluronic acid and β-D-mannuronic acid). This polymer can be regarded as a true block copolymer composed of homopolymeric regions of M (M-block) and G (G-block), interspersed within the regions of alternating structure. It also varies in composition and sequence depending on the source of the alginate. Usually, commercially available alginates are extracted from the cell wall of brown algae. In contrast to algal alginates, bacterial alginates are partially acetylated on the O-2 and O-3 positions of the mannuronate units, which protect them from conversion into guluronate by C-5 epimerase (Schmid, Messmer, Yeo, Zhang, & Zenobi, 2008). This is a possible explanation for their guluronate/mannuronate ratio, which is usually lower than in algal alginates. It has been observed that the physico-chemical properties of alginate are greatly affected by the M/G ratio as well as by the structure of the alternating zones. Alginate-based magnetic composites can be synthesized by incorporating iron oxide particles into calcium alginate hydrogel (Ma, Xiao, Li, Shi, & Zhu, 2008).

Soft magnetic materials with switching properties are prospective for biomedical applications such as; targeted drug delivery and hyperthermia. However, there are certain limitations because of their toxicity. Moreover, the applications of these nanomaterials are depending on various factors for instance, size of the particles, stability, ambient magnetic properties, and biocompatibility. In fact, the synthesis of magnetic nanoparticles (NPs) with controllable size distribution remains a great challenge for the scientist, particularly, the particle size below 10 nm which show superparamagnetic (switching) properties. Coating of these magnetic nanoparticles with biocompatible polymeric material is the area of intense research. For in vivo usage, these magnetic nanoparticles require a surface modification to ensure their non-toxic and biocompatibility for the body. Considering the hydrophobic and hydrophilic interaction the coating of different types of polymer materials has been reported (Tamhankar, Kulkarni, & Watawe, 2011 and reference therein). An efficient, economic, scalable and non-toxic synthesis of Fe_3O_4 NPs and their composites is highly desired for the potential biomedical applications and fundamental research (Liu et al., 2007).

In this paper, a facile chemical method was developed to prepare aminated-(Fe_3O_4/alginate) core/shell NCs with narrow size distributions using modified co-precipitation method. The characterization of synthesized products was done using XRD, FT-IR, RS, UV–vis, TEM, EDX and VSM techniques. The results show that the synthesized magnetic NPs are superparmagnetic in nature. The method used in the synthesis of magnetic nanoparticle is non-toxic and this approach can be used to synthesize various types of magnetic NPs.

2. Experimental

2.1. Materials

The reagent used for the preparation of Fe_3O_4 NPs and its composites with alginate, were $FeCl_2$ and $FeCl_3{\cdot}6H_2O$, trimethylamine, 75% ethanol, *Laminaria hyperborea* sodium

alginates, provided by Pronova Biopolymers Ltd. (with M_w = 60,000–80,000, and M/G = 32/68), petroleum ether, PVP and NaOH of analytical grade, purchased from Merck, New Delhi, and they were used directly without any further purification.

2.2. Synthesis of magnetic Fe_3O_4 NPs

In order to prepare Fe_3O_4 NPs by co-precipitation technique, 0.3 M aqueous solutions of $FeCl_2$ and $FeCl_3{\cdot}6H_2O$ were mixed into the ratio of 1:2. The pH of mixed solution was maintained by mixing the trimethylamine. Two different solutions were prepared for pH values 4 and 10. The mixing of trimethylamine causes the formation of precipitate in both the solutions. The obtained precipitate was filtered and washed several times to remove the impurities of chloride ions. The washed precipitate was drying in vacuum to get the final products.

2.3. Synthesis of Fe_3O_4/alg NCs

Synthesis of Fe_3O_4/alg NCs has been done following the procedure reported in the literature (Ma et al., 2008). Fig. 1 shows the preparation method of Fe_3O_4/alg NCs. In a typical procedure, a mixture of 1 g $FeCl_2$ and 50 mL 75% ethanol is added into the solution of 5 mL 2 wt% alginate–aqueous solutions and subsequently 5 mL petroleum ether was also added under vigorous magnetic stirring. Three samples at different pH (5, 9 and 14) have been synthesized by using an alkaline solution which was prepared by dissolving the 1.2 g of NaOH into 20 mL of 75% ethanol. Subsequently, the mixture is exposed to air at room temperature for 30 min. The resultant material was then filtered and washed for several time with 95% ethanol and further it was dried in air to obtain the final products.

3. Characterizations

3.1. FT-IR

The compositions of the synthesized products were examined by recording the FT-IR spectra in the spectral range of 400–4000 cm^{-1} using a model of (PerkinElmer, Spectrum BX II) spectrometer.

3.2. XRD

The phase identification and average crystallite size were investigated using powder XRD XPERT-PRO (PW3050/60) equipped with Cu-Kα radiation (λ = 1.5406 Å) operated at 30 kV and 30 mA.

3.3. Raman

Raman spectra were recorded in the range of 200–2000 cm^{-1} at room temperature, using a Renishaw inVia Raman spectrometer equipped with a high-performance CCD detector. The 514 nm line of argon-ion laser was used to illuminate the sample.

3.4. UV–vis

The optical study of the synthesized NPs was done by recording the absorption spectra in the range of 200–800 nm using UV–vis spectrophotometer (Phoenix 2200 DPCV).

3.5. TEM

The particles size of the synthesized product was investigated by HR-TEM (TEM, Tecnai G2 S-Twin) techniques.

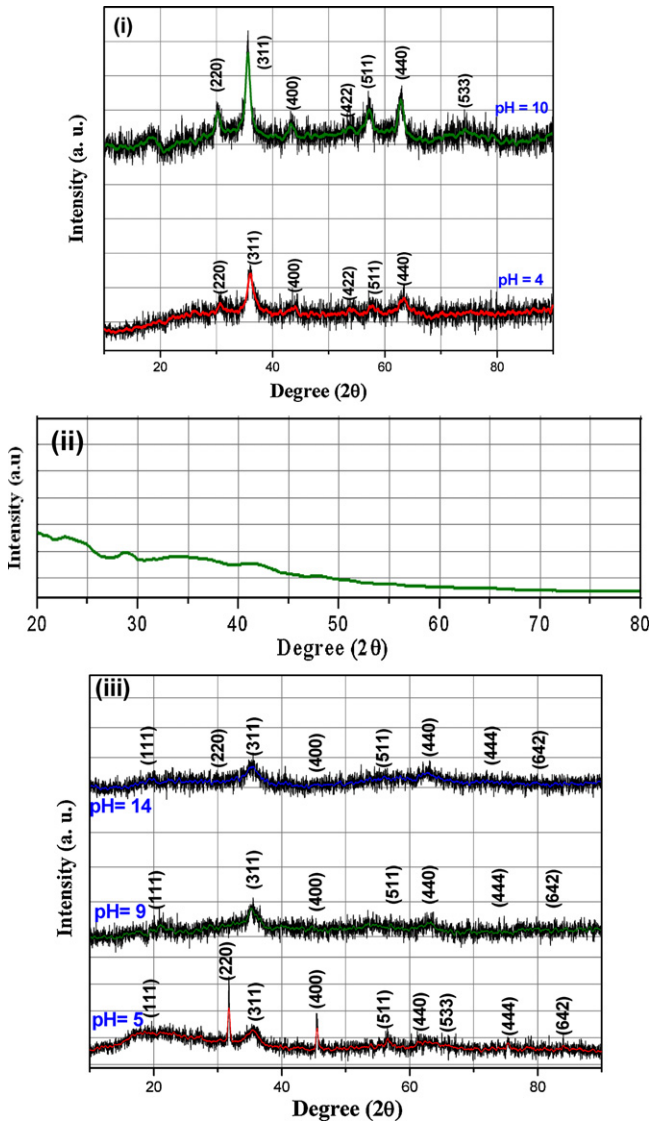

Fig. 2. XRD pattern of (i) Fe_3O_4 NPs (ii) sodium alginate and (iii) Fe_3O_4/alg NCs synthesized at different pH.

3.6. EDX

Elemental composition was investigated through energy dispersive X-ray spectroscopy (EDX) using (FEI Quanta-200 MK2).

3.7. VSM

The magnetic properties of the synthesized samples were measured at room temperature by the means of VSM (ADE-DMS, model EV-7USA) at the maximum applied field of 17.5 kOe.

4. Results and discussion

4.1. XRD study of the synthesized products

The XRD patterns of the pure Fe_3O_4 NPs synthesized by co-precipitation method are shown in Fig. 2(i). All the diffraction peaks can be indexed to the cubic and inverse type spinel structure of Fe_3O_4 with lattice constant ~a = 8.394 Å, which is in good agreement with the value obtained by JCPDS (card No. 85-1436, a = 8.393 Å). No any impurity phase was detected in the XRD patterns of the synthesized products. The appearance of broad peaks

suggests the nanocrystalline nature of Fe_3O_4 particles (Xiao et al., 2007). The average crystallite size has been calculated using Scherrer formula and the values were found to be ~10 and ~15 nm for the NPs synthesized at pH values 4 and 10, respectively.

The X-ray diffraction pattern of the sodium alginate is shown in Fig. 2(ii). No characteristic diffraction peaks were observed in the spectrum, which implies that a long range disorder along with the amorphous feature exist in sodium alginate polymer (Yu et al., 2006).

In Fig. 2(iii), the XRD patterns of Fe_3O_4/alg NCs reveal similar characteristic peaks with pure Fe_3O_4 nanoparticles, which confirm the formation of Fe_3O_4 particles. Comparing to single phase Fe_3O_4 NPs, the Fe_3O_4/alg NCs show an amorphous feature by the presence of peak at ~($2\theta = 20^\circ$) along with the low intensity of the other peaks. This is attributed to the introduction of amorphous shell of alginate (Fang, Kim, & Choi, 2009). Moreover, it is quite evident from the XRD pattern of the composites synthesized at pH value 5 that it prefers to grow along the direction of (2 2 0) plane. The mean crystallite size of synthesized Fe_3O_4/alg NCs was calculated to be ~14 nm.

4.2. FT-IR study of the synthesized products

The FT-IR spectra of Fe_3O_4 NPs and Fe_3O_4/alg NCs are presented in Fig. 3((i) and (ii)), respectively. Since Fe_3O_4 has inverse type spinel structure and it has been observed that spinel type structure exhibit mainly two absorption bands at ~600 and ~450 cm^{-1} corresponding to the metal–oxygen band in tetrahedral and octahedral sites. The FT-IR spectra of Fe_3O_4 NPs exhibit two bands around the above said wavenumber positions, which also confirm the formation of spinel type structure. In addition to it, three absorption bands in FT-IR spectra were also observed at ~3400 cm^{-1}, ~1600 cm^{-1} and ~1060 cm^{-1} which can be attributed to the stretching, bending and deformation modes, respectively due to the presence of hydroxyl group (Umare et al., 2008).

The molecular structure of alginic acid consists of two carboxylic acid moieties as shown in the synthesis scheme (see Fig. 1). The FT-IR spectra of the alginic acid and PVA functionalized Fe_3O_4/alg NCs synthesized at different pH values are shown in Fig. 3(ii). Addition of Fe_3O_4 in alginate solution shows (spectra at pH 5, 9 and 14) additional peaks in the spectral range 461–595 cm^{-1}. These peaks are attributed to the metal oxide bond (M—O) in alginate matrix. The IR bands of alginate and PVA in the spectral range 3300–3600 cm^{-1} is due to the stretching modes of OH group. The IR bands of Fe_3O_4/alg NCs become sharper and shifted to the lower wavenumber side compared to pure alginate. This indicates that OH group of alginate and PVA was involved in the assembly of Fe_3O_4 nanoparticles. Thus, M–O–M inorganic network was bonded with alginate macromolecules by hydrogen bonding as well as ionic bonding with Fe_3O_4 nanoparticles for the formation of Fe_3O_4/alg NCs. The band at ~1740 cm^{-1} can be attributed to the free carboxyl group of alginate and the band at ~1450 cm^{-1} is assigned to the symmetric COO^- stretching vibration. The C=O stretching vibration is missing in the FT-IR spectra of nanocomposites synthesized at pH 9. However, it appears at ~1740 cm^{-1} in the spectrum of pure sodium alginate and nanocomposites synthesized at pH values 5 and 14. The above discussion on the analysis of FT-IR spectra of both, Fe_3O_4 nanoparticles and Fe_3O_4/alg NCs confirms the formation of core/shell Fe_3O_4/alg nanostructures (Sergios et al., 2010).

Two different types of binding possibilities have been suggested for the surface carboxylate bonding. In one possibility, the carboxylate may be connected to the surface through one oxygen atom and both the symmetric C=O and asymmetric stretching were observed. However, in the other possibilities, the carboxylate is bound symmetrically to the surface and only symmetric C=O stretching band

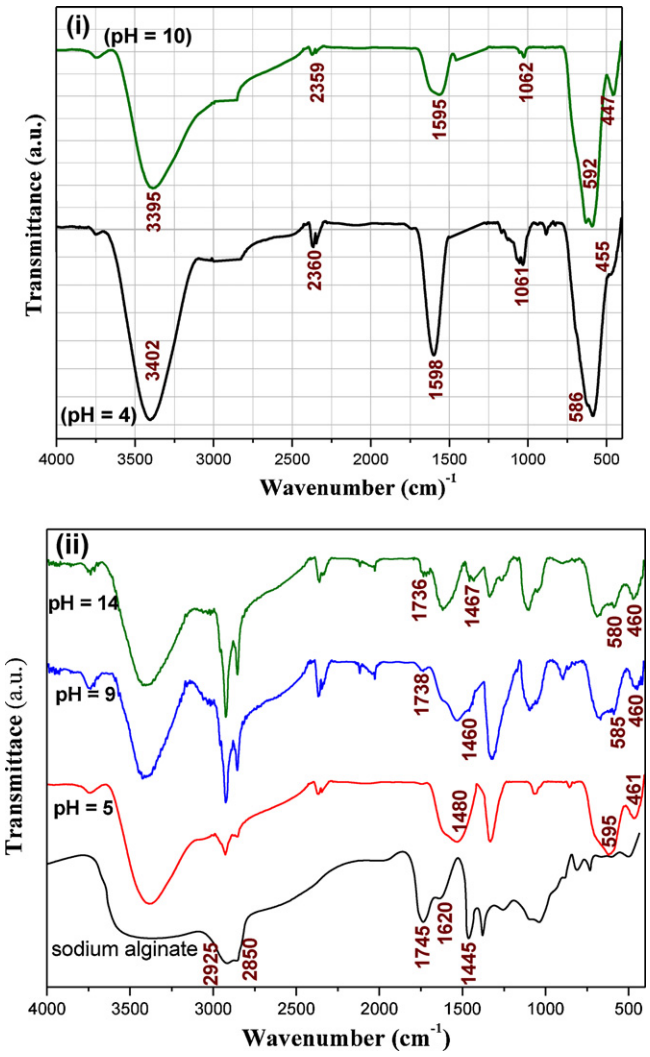

Fig. 3. FT-IR spectra of (i) Fe_3O_4 NPs and (ii) sodium alginate and Fe_3O_4/alg NCs synthesized at different pH.

appears (Unal et al., 2010) in the IR spectra. The difference in the FT-IR spectrum of the nanocomposite synthesized at pH 9 compared to the spectra of nanocomposites synthesized at pH values 5 and 14 may be due the pH dependent structural growth and modifications.

4.3. Raman study of Fe_3O_4 NPs and Fe_3O_4/alg NCs

The Raman spectra of Fe_3O_4 NPs synthesized at two different pH values 4 and 10 have been presented in Fig. 4(i). Raman spectroscopic studies on Fe_3O_4 NPs have been reported by several workers (Degiorgi, Morke, & Wachter, 1987; Gasparov et al., 2000; Gupta, Sood, Metcaff, & Honig, 2002; Shebanova & Lazor, 2003; Soler et al., 2004). In previous studies, there are some discrepancies in the observed number and positions of Raman modes. The Fe_3O_4 has spinel type structure, with 56 atoms in the unit cell and only 14 atoms in the asymmetric unit. As a result, 42 vibrational bands are expected. The analysis of group theory predicts the following vibrational bands (Fateley, Dollish, Devitt, & Bentley, 1997):

$$A_{1g} + E_g + T_{1g} + 3T_{2g} + 2A_{2u} + 2Eu + 5T_{1u} + 2T_{2u}$$

where the T_{1g}, A_{2u}, E_u and T_{2u} vibrational modes are silent in Raman spectrum and thus Fe_3O_4 exhibits only five Raman-active bands with the symmetry combination ($A_{1g} + E_g + 3T_{2g}$) and five

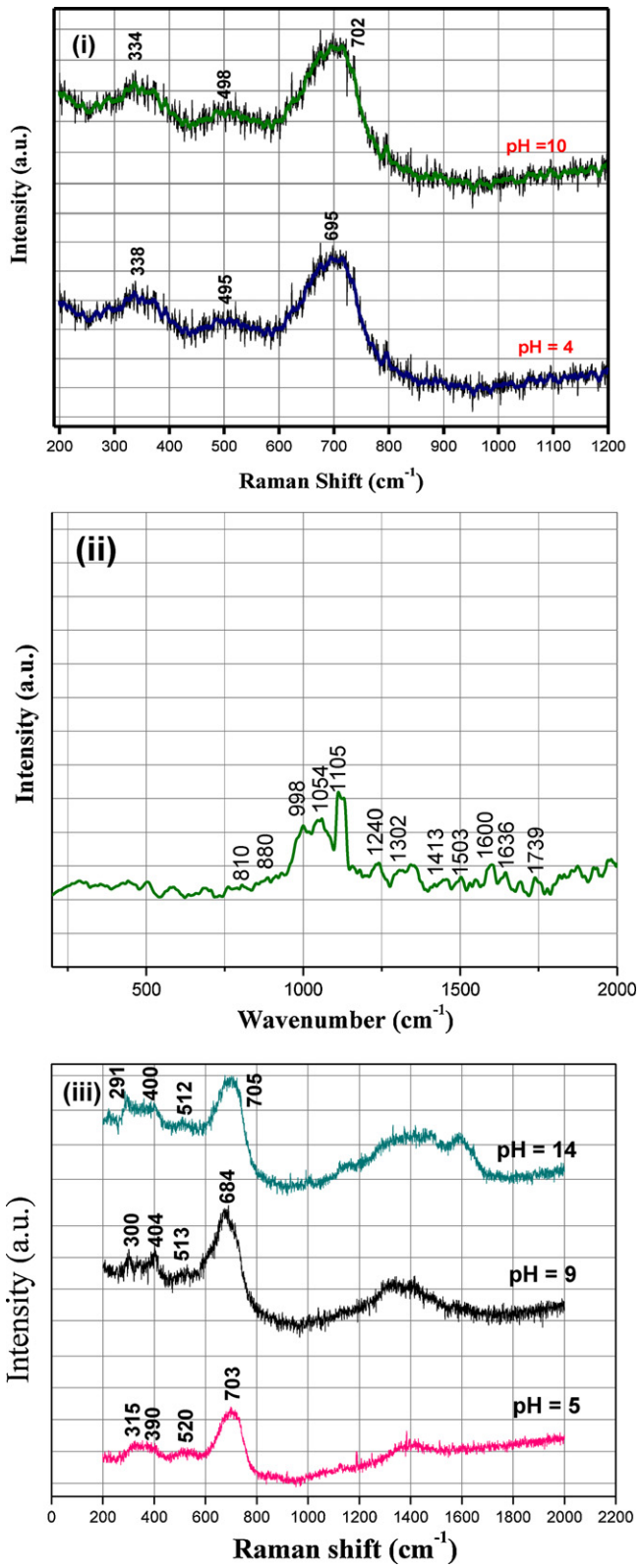

Fig. 4. Raman spectra of (i) Fe_3O_4 NPs (ii) sodium alginate and (iii) Fe_3O_4/alg NCs synthesized at different pH.

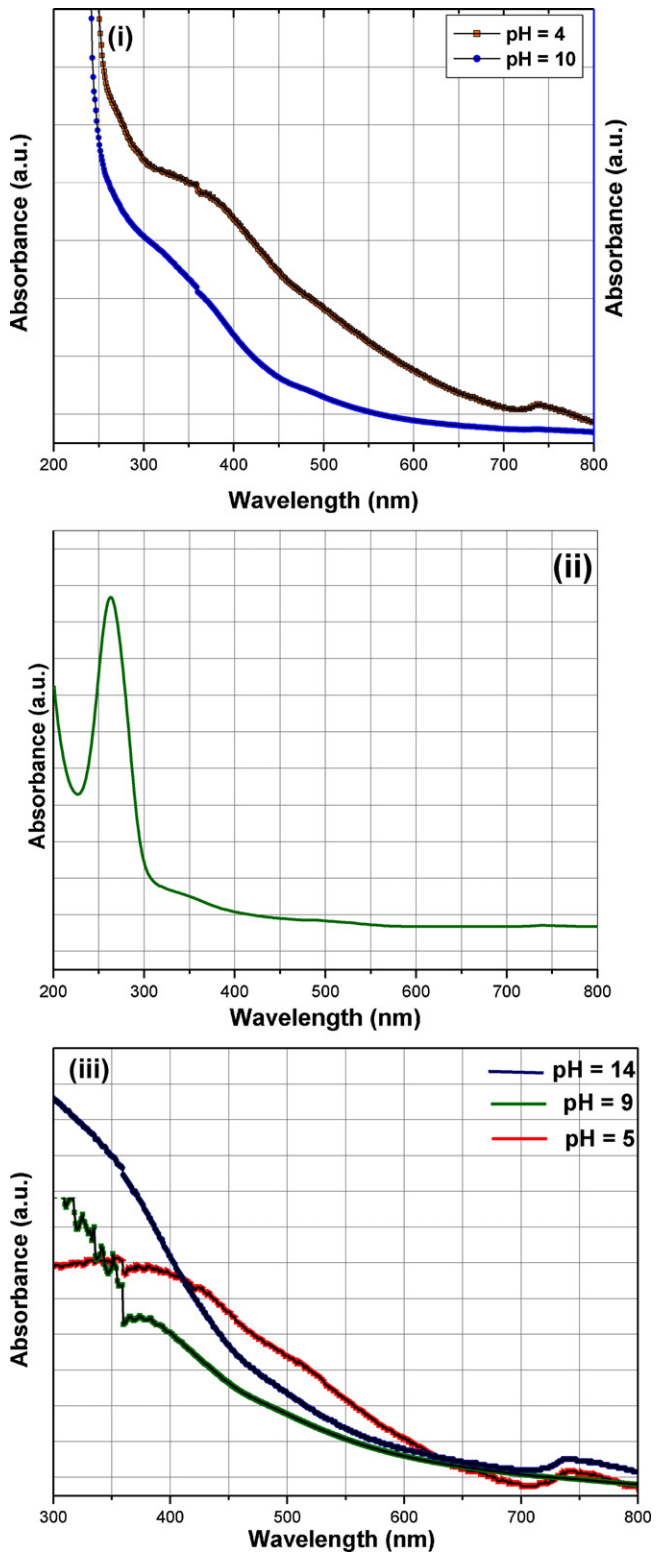

Fig. 5. UV–vis absorption spectra of (i) Fe_3O_4 NPs (ii) sodium alginate and (iii) Fe_3O_4/alg NCs synthesized at different pH.

infrared-active bands ($5T_{1u}$). In the present study, three Raman bands corresponding to the symmetry species E_g (~335), T_{2g} (~495), and A_{1g} (~695) were observed in Raman spectra of the Fe_3O_4 NPs. Fig. 4(ii) represents the Raman spectra of sodium alginate, exhibiting weak Raman vibrational modes. The most prominent bands and their assignments according to Raman spectra are shown in Fig. 4(ii). The normal Raman spectra of alginates can be divided into two parts: vibrations of the polymer backbone in the range of <1300 cm^{-1} and stretching vibrations of the carboxylate functional groups with Raman shifts at ≥1300 cm^{-1}. Interactions of alginate with sodium ions lead to band positions

with the most pronounced symmetric and asymmetric COO^- stretching vibration band at 1413 cm^{-1} and 1636 cm^{-1} respectively. The band arises at 1302 cm^{-1} is due to the stretching vibration of C—O single bond in the G/M unit of the alginate. In the range of glycosidic ring breathing modes at 1105 cm^{-1} are generally observed, which is attributed to a weakening of C—C and C—O bonds as an indirect consequence of the binding of alginate. The Raman band appears at lower wave number region at 810, 880 and 998 cm^{-1} corresponding to the skeletal of C—C, C—O stretching, and C—C—H, C—C—O bending modes respectively (Jiron, Leal, Matsuhiro, & Roman, 2009; Schmid et al., 2008; Wagner, Ivleva, Haisch, Niessner, & Horn, 2009). The Raman spectra of the Fe_3O_4/alg NCs are shown in Fig. 4(iii). We observed four Raman bands for Fe_3O_4/alg NCs with small variations in the peak positions compared to the wavenumber position of Raman bands in case of pure Fe_3O_4 nanoparticles. The position and number of observed Raman bands in case of pure Fe_3O_4 NPs and Fe_3O_4/alg NCs were found to be consistent with the earlier study (De Faria, Silva Vena uncio, & de Oliveira, 1997).

4.4. UV–vis absorption study of pure Fe_3O_4 NPs and Fe_3O_4/alg NCs

The UV–vis absorption spectra of pure Fe_3O_4 NPs, sodium alginate and Fe_3O_4/alg NCs dispersed in water solution are shown in Fig. 5(i), (ii) and (iii), respectively. The absorption spectra of pure Fe_3O_4 NPs exhibit absorption edge at ~470 nm and the optical band gap was calculated to be ~2.62 eV. The UV–vis spectrum of sodium alginate is shown in Fig. 5(ii). An intense absorption band at about ~265 nm was observed in the spectrum and it can be assigned to double bonds of alginate formed after main chain scission (Yu et al., 2006; Bhattarai & Zhang, 2007). By looking at UV–vis spectra (Fig. 5(i) and (iii)) one can easily notice an obvious difference between the absorbance spectra of pure Fe_3O_4 and Fe_3O_4/alg NCs. It indicates that Fe_3O_4 nanoparticles interact with the alginate molecules. The observed results were found to be comparable with the earlier study (Zhang, Niu, Cai, & Shi, 2010).

4.5. TEM investigation of Fe_3O_4 NPs and Fe_3O_4/alg NCs

The TEM micrographs of Fe_3O_4 NPs synthesized at pH 10 and 4 are shown in Fig. 6((i), a and b), respectively. The Fe_3O_4 NPs synthesized at pH 10 shows some extent of agglomeration. However, the Fe_3O_4 NPs synthesized at pH 4 shows better dispersion. The average particle size for the particles synthesized at pH 4 was calculated to be ~8.5 nm with help of the distribution curve fitted with Lorentzian function and shown in Fig. 6(c). TEM micrographs of the Fe_3O_4/alg NCs are presented in Fig. 6(ii), (iii) and (iv). TEM images of Fe_3O_4/alg NCs show a better dispersion of the particles in comparison to that of pure Fe_3O_4 NPs and it may be due to the coating of alginate on the surface of the Fe_3O_4 NPs, which essentially reduces the interaction between the magnetic NPs and finally resulting a better dispersion of the nanoparticles. The average size of the nanocomposites synthesized at pH 14 was also calculated by distribution curve and found to be ~10.5 nm. The distribution curve is shown in Fig. 6((iv) b). The HR-TEM images of the Fe_3O_4/alg NCs synthesized at different pH exhibit core/shell (Fe_3O_4/alginate) type nanostructures. The SAED patterns of Fe_3O_4/alg NPs exhibit bright rings which suggest the polycrystalline nature of Fe_3O_4/alg NCs (see Fig. 6((ii) a). In order to determine the composition of (Fe_3O_4/alg NCs), synthesized at different pH value EDX, investigations were also performed. Fig. 6(v) shows EDX pattern of the (Fe_3O_4/alg NCs) synthesized at different pH value. The EDX analysis reveal that the wt% of Fe was highest when (Fe_3O_4/alg NCs) was synthesized at pH 5, whereas it was found to be minimum when the synthesis was done at pH 14. The difference in the composition may due to the response of the chemical reaction at different pH during the synthesis processes, which also influences the degree of polymerization/combination of magnetic nanoparticle.

Table 1
Magnetic properties of the Fe_3O_4 nanoparticles and Fe_3O_4/alginate nanocomposites.

Sample	Saturation magnetization M_s (emu/g)
Fe_3O_4 nanoparticles synthesized at pH 4	31.03
Fe_3O_4 nanoparticles synthesized at pH 10	35.57
Fe_3O_4/alginate nanocomposites synthesized at pH 5	5.40
Fe_3O_4/alginate nanocomposites synthesized at pH 9	4.69
Fe_3O_4/alginate nanocomposites synthesized at pH 14	2.35

4.6. Magnetic properties of pure Fe_3O_4 NPs and Fe_3O_4/alg NCs

The typical magnetization curves of the Fe_3O_4 nanoparticle and Fe_3O_4/alg NCs are shown in Fig. 7(i) and (iii), respectively. The M–H curve was obtained in the presence of magnetic field of 17.5 kOe at the room temperature. In this study, we observed that the Fe_3O_4 nanoparticle and Fe_3O_4/alg NCs exhibit neither coercivity (H_c) nor remanent magnetization (M_r), which proves that both, Fe_3O_4 nanoparticle and Fe_3O_4/alg NCs are superparamagnetic in nature. Moreover, the M–H curve do not saturate up to the maximum applied field. The values of saturation magnetization (M_s) at the maximum filed are given in Table 1. The reason for superparamagnetic nature of the NPs is essentially due to the very small size. The smaller size (see Fig. 6) may be considered as equivalent to a single magnetic domain where the energy barrier for its spin reversal easily overcomes by thermal vibrations resulting superparamagnetic nature of nano size particles. Further, Morrish and Yu (1955) have reported that Fe_3O_4 NPs having particle size ~50 nm or even less may be considered as a single domain.

The values of M_s of the Fe_3O_4 NPs were found to be 31.03 emu/g and 33.58 emu/g for the Fe_3O_4 nanoparticles synthesized at pH values 4 and 10, respectively. The difference in the values of M_s may be attributed to difference in their size and structural morphology of the Fe_3O_4 NPs. For a comparative study, we also characterized sodium alginate through VSM technique. The M–H loop measured at room (Fig. 7(ii)) temperature exhibit diamagnetic characteristics of the sodium alginate. On the other hand, the values of M_s for Fe_3O_4/alg NCs were found to be decreasing by increasing the pH value (see Table 1). It was reported that the magnetic properties of the composites depend upon the content of Fe_3O_4 NPs (Luo et al., 2010) in the Fe_3O_4/alg matrix. On the basis of above discussion on the pH dependent changes in the M_s of the synthesized nanocomposites; we may conclude that by increasing the pH of the solution causes low concentration of Fe_3O_4 NPs in the alginate matrix which essentially reduce the value of M_s of the Fe_3O_4/alg nanocomposites. Thus we found that the change in magnetic properties of the synthesized samples is highly affected due to the change in pH values during the synthesis process, which essentially influence the rate of the chemical reactions causing a significant modification in the structure and composition of the synthesized products consequently the magnetic properties of the products. Decrease in saturation magnetization of the Fe_3O_4/alg nanocomposites is also supported by the EDX results because of decreasing wt% of Fe on

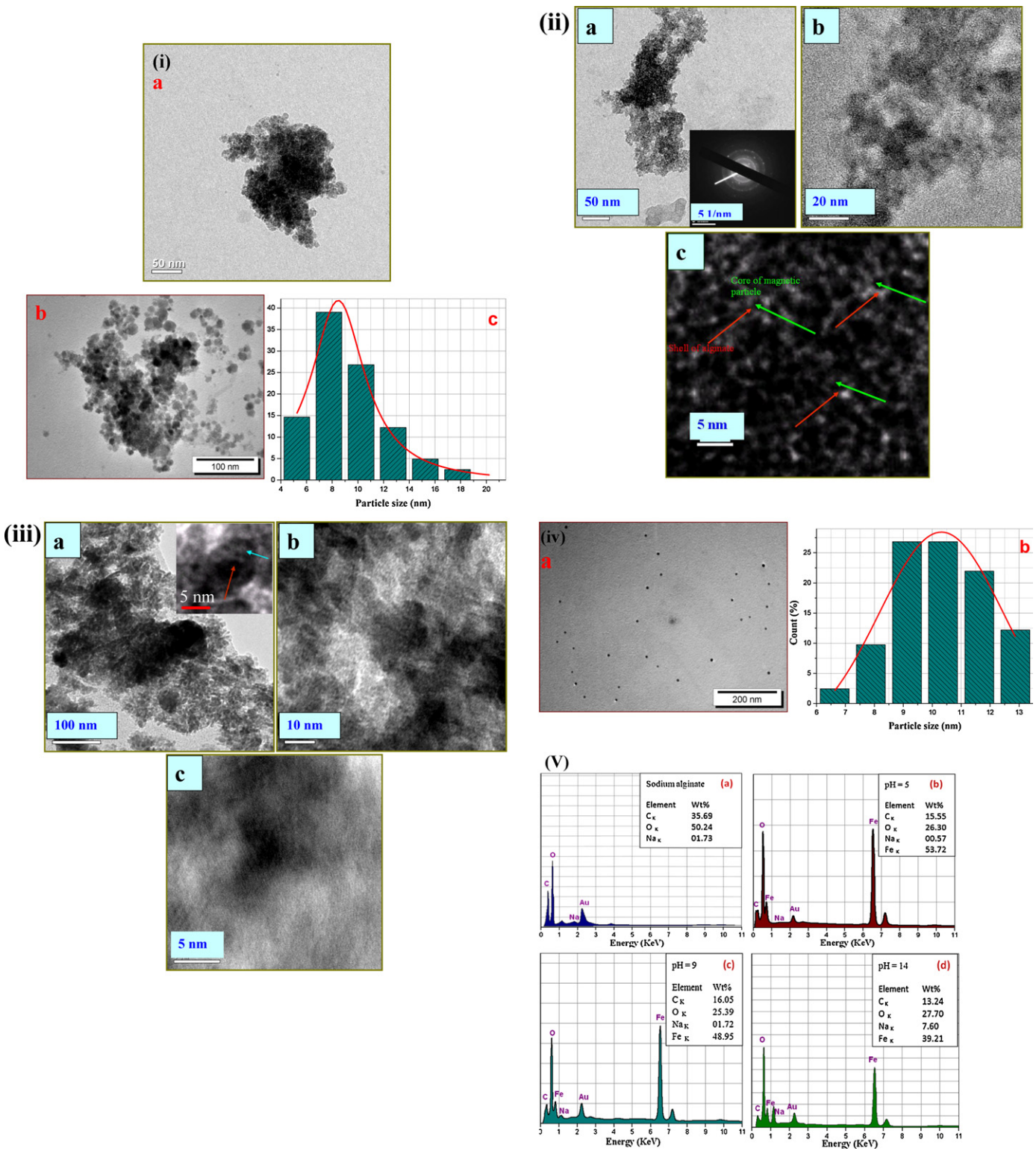

Fig. 6. TEM micrograph of (i) (a) Fe_3O_4 NPs synthesized at pH, 10 (b) TEM micrograph of the nanoparticles synthesized at pH, 4 (c) Particle size distribution curve of the nanoparticles synthesized at pH, 4 (ii) (a–c) Fe_3O_4/alg NCs synthesized at pH, 5 The inset of (ii-a) is the SAED pattern of the nanocomposites (ii-c) exhibit the core of Fe_3O_4 and alginate as the shell (iii) (a–c) is the TEM micrograph of the nanocomposites synthesized at pH, 9. Inset of (iii-a) exhibit the core of Fe_3O_4 (dark image) and alginate as the shell (in light image). Part (iii-c) is the HR-TEM images of the nanocomposites and (iv) (a) TEM micrograph of the Fe_3O_4/alg NCs synthesized at pH, 14 (b) Particle size distribution curve of the Fe_3O_4/alg NCs synthesized at pH, 14 and (v) EDX pattern of sodium alginate (a) and Fe_3O_4/alg NCs synthesized at different pH (b–d).

increasing the pH value. The variations in magnetic properties have been also observed when the products were synthesized at different pH value (Srivastava, Ojha, Chaubey, Sharma, & Pandey, 2010; Wu, Huang, Wang, & Wu, 2005; Zhang, Shi, et al., 2010; Zhang, Niu, et al., 2010). The synthesized superparamagnetic NPs may be used in various types of biomedical applications because of the superparmagnetic properties (exhibit switching properties), highly desirable for in vivo applications.

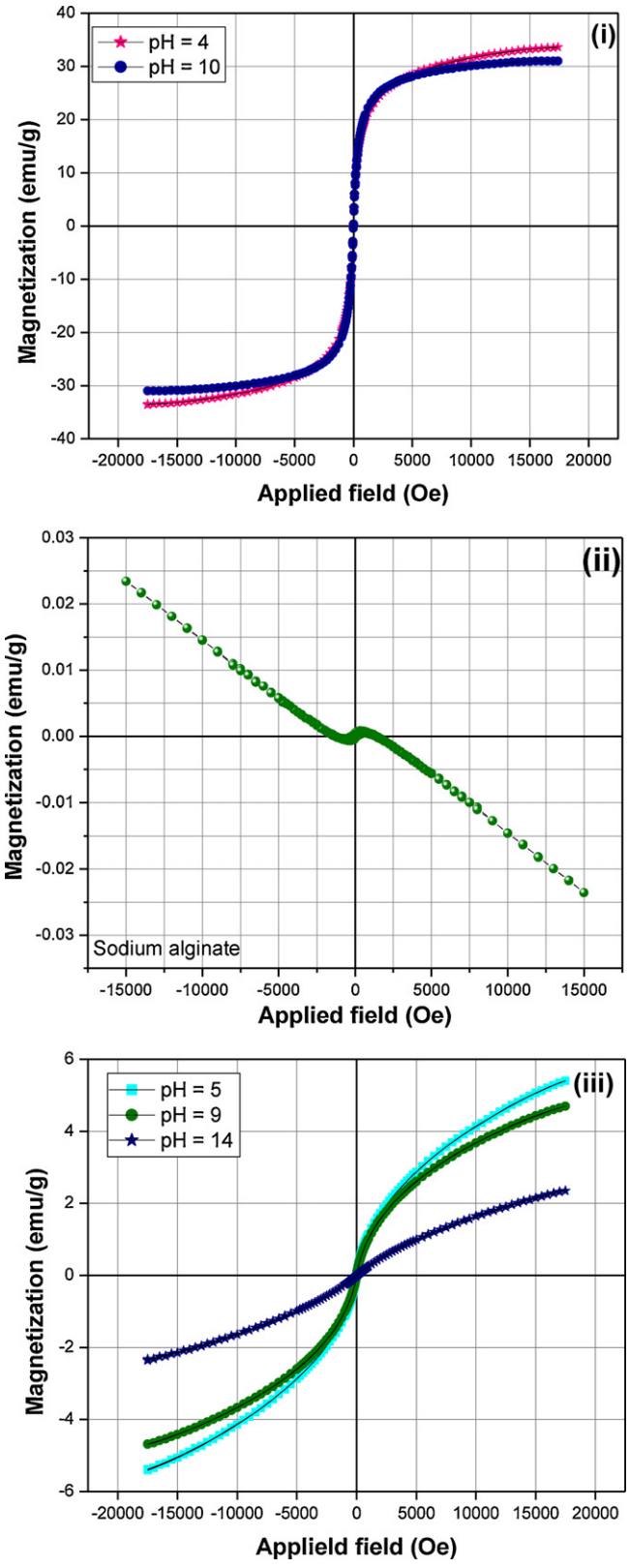

Fig. 7. M–H curve of (i) Fe_3O_4 NPs (ii) sodium alginate and (ii) Fe_3O_4/alg NCs synthesized at different pH.

5. Conclusions

In conclusion, superparamagnetic Fe_3O_4 nanoparticle and Fe_3O_4/alg NCs were synthesized by co-precipitation and in situ co-precipitation assisted polymerization methods, respectively. TEM micrographs show that Fe_3O_4 NPs were wrapped by a layer of alginate molecules indicating the formation of core/shell (Fe_3O_4/alginate) type nanostructures. Magnetization measurements show that the synthesized products are superparamagnetic in nature at room temperature. The value of saturation magnetization in the case of Fe_3O_4/alg NCs decreases by increasing the pH values. The synthesized superparamagnetic NPs and its composite with biocompatible alginate can be used in various types of biomedical applications.

Acknowledgments

MS is thankful to MNNIT, Allahabad for granting the senior research fellowship. JS is thankful to CSIR, India for the award of research associateship. AKO is thankful to the Alexander von Humboldt Stiftung for the award of a research fellowship. The Department of Chemistry of MNNIT, Allahabad is gratefully acknowledged for granting access to the available research facilities. Electron Microscope Facility, Department of Anatomy Institute of Medical Sciences, Banaras Hindu University, Varanasi is highly acknowledged for providing the TEM facility.

References

Bhattarai, N., & Zhang, M. (2007). Controlled synthesis and structural stability of alginate-based nanofibers. *Nanotechnology*, *18*, 455601–455610.

De Faria, D. L. A., Silva Venâncio, S., & de Oliveira, M. T. (1997). Raman microspectroscopy of some iron oxides and oxyhydroxides. *Journal of Raman Spectroscopy*, *28*, 873–878.

Degiorgi, L., Morke, I. B., & Wachter, P. (1987). Magnetite: Phonon modes and the Verwey transition. *Physical Review B*, *35*, 5421–5424.

Fang, F. F., Kim, J. H., & Choi, H. J. (2009). Synthesis of core–shell structured PS/Fe_3O_4 microbeads and their magnetorheology. *Polymer*, *50*(10), 2290–2293.

Fateley, W. G., Dollish, F. R., Devitt, N. T. M., & Bentley, F. F. (1997). *Infrared and Raman selection rules for molecular and lattice vibrations: The correlation method*. New York: John Wiley and Sons, Inc., p. 169.

Gasparov, L. V., Tanner, D. B., Romero, D. B., Berger, H., Margaritondo, G., & Forro, L. (2000). Infrared and Raman studies of the Verwey transition in magnetite. *Physical Review B*, *62*, 7939–7944.

Gupta, A. K., & Gupta, M. (2005). Synthesis and surface engineering of iron oxide nanoparticles for biomedical applications. *Biomaterials*, *26*(18), 3995–4021.

Gupta, R., Sood, A. K., Metcaff, P., & Honig, J. M. (2002). Raman study of stoichiometric and Zn-doped Fe_3O_4. *Physical Review B*, *65*, 104430–104437.

Jiron, G. C., Leal, D., Matsuhiro, B., & Roman, I. O. O. (2009). Vibrational spectroscopy and density functional theory calculations of poly-D-mannuronate and heteropolymeric fractions from sodium alginate. *Journal of Raman Spectroscopy*, *42*, 870–878.

Kim, G. C., Li, Y. Y., Chu, Y. F., Cheng, S. X., Zhuo, R. X., & Zhang, X. Z. (2008). Nanosized temperature-responsive Fe_3O_4-UA-*g*-P(UA-*co*-NIPAAm) magnetomicelles for controlled drug release. *European Polymer Journal*, *44*(9), 2761–2767.

Li, G., Jiang, Y., Huang, K., Ding, P., & Chen, J. (2008). Preparation and properties of magnetic Fe_3O_4–chitosan nanoparticles. *Journal of Alloys and Compounds*, *466*(1–2), 451–456.

Liu, H. L., Ko, S. P., Wu, J. H., Jung, M. H., Min, J. H., Lee, J. H., et al. (2007). One-pot polyol synthesis of monosize PVP-coated sub-5 nm Fe_3O_4 nanoparticles for biomedical applications. *Journal of Magnetism and Magnetic Materials*, *310*(2), e815–e817.

Liu, J., Zhang, Y., Yang, T., Ge, Y., Zhang, S., Chen, Z., et al. (2009). Synthesis, characterization and application of composite alginate microspheres with magnetic and fluorescent functionalities. *Journal of Applied Polymer Science*, *113*, 4042–4051.

Liu, T. Y., Hu, S. H., Liu, K. H., Liu, D. M., & Chen, S. Y. (2008). Study on controlled drug permeation of magnetic-sensitive ferrogels: Effect of Fe_3O_4 and PVA. *Journal of Controlled Release*, *126*(3), 228–236.

Luo, Y. L., Fan, L. H., Xu, F., Chen, Y. S., Zhang, C. H., & Wei, Q. B. (2010). Synthesis and characterization of Fe_3O_4/PPy/P(MAA-co-AAm) trilayered composite microspheres with electric, magnetic and pH response characteristics. *Materials Chemistry and Physics*, *120*(2-3), 590–597.

Ma, P., Xiao, C., Li, L., Shi, H., & Zhu, M. (2008). Facile preparation of ferromagnetic alginate-*g*-poly(vinyl alcohol) microparticles. *European Polymer Journal*, *44*(11), 3886–3889.

Morrish, A. H., & Yu, S. P. (1955). Dependence of the coercive force on the density of some iron oxide powders. *Journal of Applied Physics*, *26*, 1049–1055.

Pielesz, A. (2007). Raman spectroscopy as a tool for analysing dye distribution in alginate hydrogels. *Fibers and Textiles in Eastern Europe*, *15*, 64–65.

Qu, J., Liu, G., Wang, Y., & Hong, R. (2010). Preparation of Fe_3O_4–chitosan nanoparticles used for hyperthermia. *Advanced Powder Technology*, *21*(4), 461–467.

Schmid, T., Messmer, M., Yeo, B. S., Zhang, W., & Zenobi, R. (2008). Towards chemical analysis of nanostructures in biofilms II: Tip-enhanced Raman spectroscopy of alginates. *Analytical and Bioanalytical Chemistry*, *391*, 1907–1916.

Sergios, K., Papageorgiou, E. P., Kouvelos, E. P., Favvas, A. A. S., George, E. R., & Fotios, K. K. (2010). Metal–carboxylate interactions in metal–alginate complexes studied with FTIR spectroscopy. *Carbohydrate Research*, *345*(4), 469–473.

Shebanova, O. N., & Lazor, P. (2003). Raman spectroscopic study of magnetite ($FeFe_2O_4$): A new assignment for the vibrational spectrum. *Journal of Solid State Chemistry*, *174*(2), 424–430.

Singh, J., Kalita, P., Singh, M. K., & Malhotra, B. D. (2011). Nanostructured nickel oxide-chitosan film for application to cholesterol sensor. *Applied Physics Letters*, *98*, 123702–123704.

Singh, J., Srivastava, M., Dutta, J., & Dutta, P. K. (2011). Preparation and properties of hybrid monodispersed magnetic α-Fe_2O_3 based chitosan nanocomposite film for industrial and biomedical applications. *International Journal of Biological Macromolecules*, *48*(1), 170–176.

Soler, M. A. G., Melo, T. F. O., Silva, S. W., Lima, E. C. D., Pimenta, A. C. M., Garg, V. K., et al. (2004). Structural stability study of cobalt ferrite-based nanoparticle using micro Raman Spectroscopy. *Journal of Magnetism and Magnetic Materials*, *272–276*(3), 2357–2358.

Srivastava, M., Ojha, A. K., Chaubey, S., Sharma, P. K., & Pandey, A. C. (2010). Influence of pH on structural morphology and magnetic properties of ordered phase cobalt doped lithium ferrites nanoparticles synthesized by sol–gel method. *Materials Science and Engineering B*, *175*(1), 14–21.

Sun, H., Zhu, X., Zhang, L., Zhang, Y., & Wang, D. (2010). Capture and release of genomic DNA by PEI modified Fe_3O_4/Au nanoparticles. *Materials Science and Engineering C*, *30*(2), 311–315.

Tamhankar, M. P., Kulkarni, A. M., & Watawe, S. C. (2011). Functionalization of cobalt ferrite nanoparticles with alginate coating for biocompatible applications. *Materials Sciences and Applications*, *2*, 1317–1321.

Umare, S. S., Ningthoujam, R. S., Sharma, S. J., Shrivastava, S., Kurian, S., & Gajbhiye, N. S. (2008). Mössbauer and magnetic studies on nanocrystalline $NiFe_2O_4$ particles prepared by ethylene glycol route. *Hyperfine Interact*, *184*(1–3), 235–243.

Unal, B., Toprak, M. S., Durmus, Z., Sözeri, H., & Baykal, A. (2010). Synthesis, structural and conductivity characterization of alginic acid–Fe_3O_4 nanocomposite. *Journal of Nanoparticle Research*, *12*(8), 3039–3048.

Wagner, M., Ivleva, N. P., Haisch, C., Niessner, R., & Horn, H. (2009). Combined use of confocal laser scanning microscopy (CLSM) and Raman microscopy (RM): Investigations on EPS–matrix. *Water Research*, *43*, 63–76.

Wang, S., Bao, H., Yang, P., & Chen, G. (2008). Immobilization of trypsin in polyaniline-coated nano-Fe_3O_4/carbon nanotube composite for protein digestion. *Analytica Chimica Acta*, *612*(2), 182–189.

Wang, S., Tan, Y., Zhao, D., & Liu, G. (2008). Amperometric tyrosinase biosensor based on Fe_3O_4 nanoparticles–chitosan nanocomposite. *Biosensors and Bioelectronics*, *23*(12), 1781–1787.

Wu, K. H., Huang, W. C., Wang, G. P., & Wu, T. R. (2005). Effect of pH on the magnetic and dielectric properties of SiO_2/NiZn ferrite nanocomposites. *Materials Research Bulletin*, *40*(10), 1822–1831.

Xiao, Q., Tan, X., Ji, L., & Xue, J. (2007). Preparation and characterization of polyaniline/nano-Fe_3O_4 composites via a novel Pickering emulsion route. *Synthetic Metals*, *157*(18–20), 784–791.

Yang, T., Brown, R. N. C., Kempel, L. C., & Kofinas, P. (2008). Magneto-dielectric properties of polymer–Fe_3O_4 nanocomposites. *Journal of Magnetism and Magnetic Materials*, *320*(21), 2714–2720.

Yu, Y., Zhihuai, S., Chen, S., Bian, C., Chen, W., & Xue, G. (2006). Facile synthesis of polyaniline-sodium alginate nanofibers. *Langmuir*, *22*, 3899–3905.

Zhang, C., Shi, J., Yang, X., De, L., & Wang, X. (2010). Effects of calcination temperature and solution pH value on the structural and magnetic properties of $Ba_2Co_2Fe_{12}O_{22}$ ferrite via EDTA-complexing process. *Materials Chemistry and Physics*, *123*(2-3), 551–556.

Zhang, S., Niu, H., Cai, Y., & Shi, Y. (2010). Barium alginate caged Fe_3O_4@C18 magnetic nanoparticles for the pre-concentration of polycyclic aromatic hydrocarbons and phthalate esters from environmental water samples. *Analytica Chimica Acta*, *665*(2), 167–175.